(Received 3 June 2025, Accepted 5 August 2025, Scheduled 14 August 2025)

Design of UWB Monopole Antenna with Ring Structure Based on Characteristic Mode Theory

Zhen Xiang[1], Zhonggen Wang[1,*], Chenlu Li[2], and Rui You[1]

[1]*School of Electrical and Information Engineering, Anhui University of Science and Technology, Huainan 232001, China*
[2]*School Electrical and Information Engineering, Hefei Normal University, Hefei 230061, China*

ABSTRACT: In this paper, an ultra-wideband monopole antenna for wireless communication is designed and fabricated based on characteristic mode theory. The antenna is mainly composed of a metal main body and a circular metal patch, and the antenna dimensions are $35 \times 30 \times 1.6\,\text{mm}^3$. In order to enhance its matching performance, a circular groove is made in the center of the circular metal patch, and an outer ring is added to the outside. In order to expand the covered bandwidth and reduce the reflection loss, an isosceles right triangle is cut off from each side of the ground plane. The length of the ground plane and the side length of the ground plane cut angle are optimized. The key modes are determined through the analysis of the characteristic mode theory. The simulation and measurement results show that this antenna covers the frequency band of 3.03–11.75 GHz, with a maximum return loss of -42.26 dB and excellent radiation performance.

1. INTRODUCTION

Monopole antenna, as a fundamental structure in the field of electromagnetic radiation, has witnessed the evolution of radio technology. Since its birth in the early 20th century, it has become a core component of early wireless systems due to its simple structure, low cost, and easy matching and optimization. Although modern communication has given rise to many new types of antennas, its omnidirectional radiation characteristics remain irreplaceable in key fields such as mobile communication base stations, maritime navigation, and microwave remote sensing [1–3].

The monopole antenna's omnidirectional radiation pattern provides significant advantages for wide-coverage applications, including Internet of Things (IoT) terminals and vehicle communication systems. Its theoretical characteristic impedance of 36.5 Ω achieves good impedance matching with standard 50 Ω transmission lines, effectively mitigating standing wave losses and improving system energy efficiency [4, 5]. Based on the aforementioned various advantages of the monopole antenna, many studies have been conducted on this topic [6–13]. In [8], a miniaturized broadband circularly polarized antenna operating in the ultra-high frequency band is designed, using closely coupled monopole radiation units and a double-layer broadband sequential feed network. Through the rotation optimization of the radiation elements, the stability of the full-frequency band radiation pattern and beamwidth was ensured. In [11], a new type of printed monopole antenna composed of a superstructure and two arms to regulate the ground current is proposed, achieving the stability of the radiation pattern and the optimization of impedance matching. It obtained the working bandwidth ($S_{11} < -10$ dB) at the lowest frequency wavelength.

Among various monopole antennas, ultra-wideband (UWB) antennas have been widely studied due to their wide coverage frequency band, high transmission rate, and low latency. The technology applied to it is UWB technology [14, 15]. However, the design of UWB antennas still includes challenges such as wide impedance matching, radiation stability, low profile, compact size, and low cost [16–18]. Therefore, many scholars have conducted extensive research on UWB monopole antennas [19–26]. In [20], a low-profile compact UWB monopole antenna is designed, combining a metal wire coil with a meandering dipole structure, achieving 900 MHz global system for mobile (GSM) communication frequency band and ultra-4 GHz wideband coverage. In [23], a UWB patch antenna is fabricated through the innovation of conductive adhesive process. Compared with the traditional copper-layer antenna, the bandwidth is optimized by 200%, covering the ultra-wide frequency band from 609 MHz to 9.105 GHz.

From the above research, it can be observed that when being combined with UWB technology, by optimizing the geometric topology and dielectric parameters of the antenna, an improved structure covering the ultra-wide frequency band of 3.1–10.6 GHz can be constructed. This solution retains the advantages of UWB, such as high throughput and low power consumption, and through structural innovation, it achieves frequency band expansion, providing an effective hardware solution for short-range high-speed communication systems [26].

In the aforementioned references, traditional antenna design mostly relies on the personal experience of the designer and lacks systematic theoretical support. In recent years, characteristic mode analysis (CMA) theory has emerged as a core

* Corresponding author: Zhonggen Wang (zgwang@ahu.edu.cn).

method for modern antenna design. By studying the current distribution of the antenna's intrinsic mode in the unexcited state, it analyzes the radiation behavior from a physical perspective [27–29]. By optimizing the characteristic mode to design an appropriate feeding method to excite the required characteristic mode of the antenna, the initial design goal and performance indicators of the antenna can be achieved [30–33]. Therefore, using the characteristic mode theory to design antennas is also a popular approach at present, and a large number of references have conducted research on this [34–37]. In [34], a new type of tri-frequency microstrip superstructure (MTS) circularly polarized antenna was designed based on CMA, achieving circular polarization radiation in three frequency bands of 7.75 GHz, 8.8 GHz, and 9.8 GHz. In [36], a broadband omnidirectional antenna is proposed based on characteristic mode theory, achieving a 44.2% wide impedance bandwidth (1.85–2.9 GHz, $S_{11} < -10$ dB) and stable omnidirectional radiation mode across the entire frequency range.

Due to the numerous advantages of UWB technology, many research papers have combined the characteristic mode theory with UWB technology to design antennas [38–40]. Ref. [38] analyzes a UWB monopole antenna based on characteristic mode theory, revealing the mechanism of achieving UWB by superimposing characteristic modes through comparing the modal characteristics of asymmetric dipoles and broadband monopoles. The working frequency band covers 2.8 GHz to above 10 GHz ($S_{11} < -10$ dB).

Based on this, this paper designs a UWB monopole antenna using characteristic mode theory. The designed UWB monopole antenna is simulated and measured. The results show that the frequency band range covered by the antenna designed is 3.03–11.75 GHz; the lowest return loss is −42.26 dB; and the radiation performance is good, which can be used in wireless communication systems.

2. ANTENNA STRUCTURE

2.1. Antenna Composition

The antenna comprises a metal main body and a circular patch. To enhance impedance matching, a central circular slot is etched within the patch, and an outer annular ring is added. The ground plane adopts a rectangular structure. To further increase impedance matching and expand the frequency band covered by the antenna, the length of the ground plane is studied and optimized. At the same time, an isosceles right triangle is opened on each side of the ground plane, and the length of its right-angle side is optimized. The values at which they achieve the best performance are given.

2.2. Antenna-Related Parameters

Figure 1 presents the structure and parameters of the UWB antenna proposed in this paper. The antenna has a size of $35 \times 30 \times 1.6\,\text{mm}^3$, and the substrate is fabricated from FR4 dielectric material, with a relative permittivity of 4.4 and a loss tangent of 0.02. The patch is composed of a main body and a circular ring sleeve. The width of the main body part is $W_2 = 2$ mm, and the length is $L_2 = 12.4$ mm. The radius

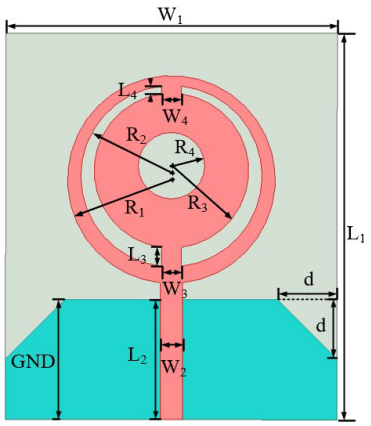

FIGURE 1. The diagram of UWB antenna structure.

of the outer circle of the circular ring sleeve is $R_1 = 9.4$ mm; the radius of the hollow ring formed at the center of the sleeve is $R_2 = 8.2$ mm; and the radius of the inner circle formed inside the sleeve is $R_3 = 7$ mm. A circular slot with a radius of $R_4 = 3$ mm is opened at its center. The widths of the two rectangles connecting the upper and lower parts of the circular ring sleeve are both 1.8 mm, and their lengths are $W_4 = 0.7$ mm and $W_3 = 1.7$ mm, respectively. The width of the ground plane is $W_1 = 30$ mm, and the length is $GND = 10.9$ mm. An isosceles right triangle is truncated on each of the left and right sides, with the length of the right-angle side being d. The final dimensions of the optimized antenna are presented in Table 1.

TABLE 1. Dimensions of the UWB antenna (unit: mm).

Parameters	L_1	W_1	L_2	W_2	L_3	W_3	L_4
Value	35	30	12.4	2	1.7	1.8	0.7
Parameters	W_4	R_1	R_2	R_3	R_4	d	GND
Value	1.8	9.4	8.2	7	3	5.4	10.9

3. ANTENNA OPTIMIZATION PROCESS AND ANALYSIS

3.1. Optimization Process

Figure 2 presents the optimization process of the UWB monopole antenna, adopting the microstrip line feeding approach. The model is constructed using the electromagnetic simulation software HFSS, where boundary conditions and excitation are set. After establishing the sweep frequency, the simulation is carried out. The HFSS model post-simulation is imported into the 3D electromagnetic field simulation software CST for characteristic mode analysis to obtain the mode current distribution of the antenna, as depicted in Figure 3. During the analysis of the antenna using characteristic mode theory, modal significance (MS) is a highly significant parameter, with the calculation formula being as follows. When MS is greater than 0.707, it indicates that this mode can be readily excited; conversely, when MS approaches 0, it is difficult to excite. Characteristic mode analysis is conducted on (a) in Figure 2, namely Ant 1, and the MS curve is obtained as shown in Figure 4.

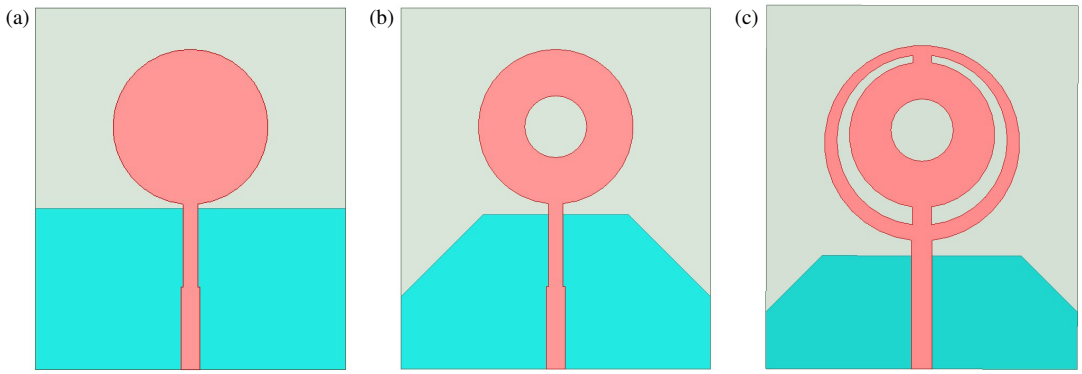

FIGURE 2. Optimization process of antenna structure: (a) Ant 1, (b) Ant 2, (c) Ant 3.

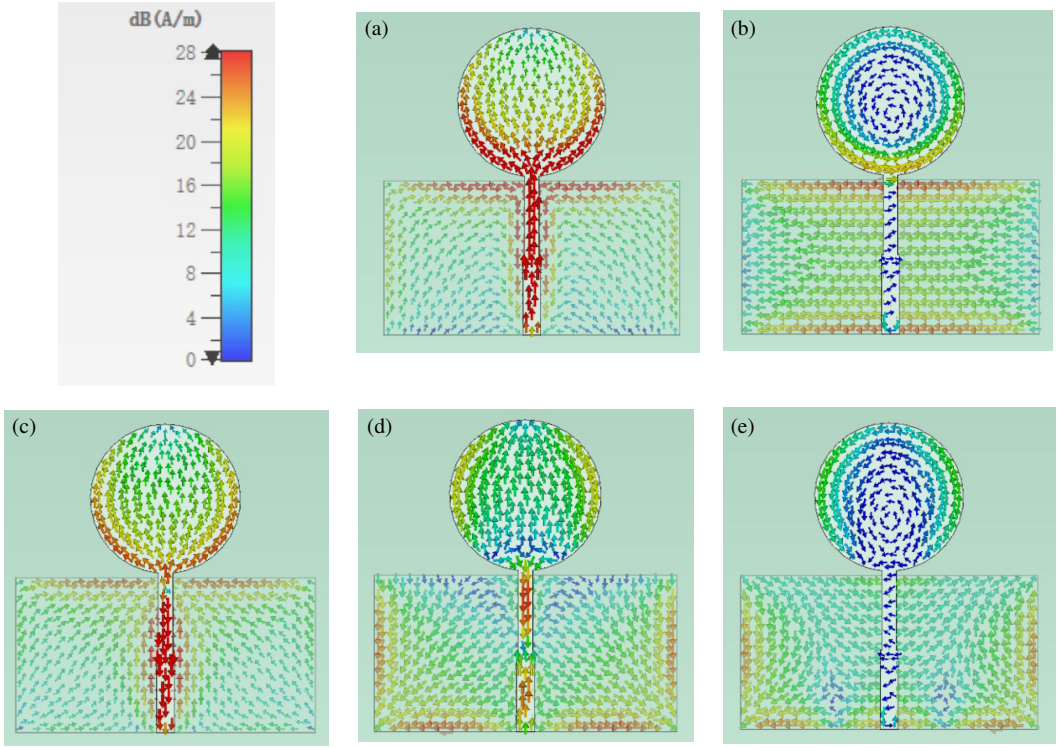

FIGURE 3. Mode current distribution of Ant 1: (a) mode 1, (b) mode 2, (c) mode 3, (d) mode 4, (e) mode 5.

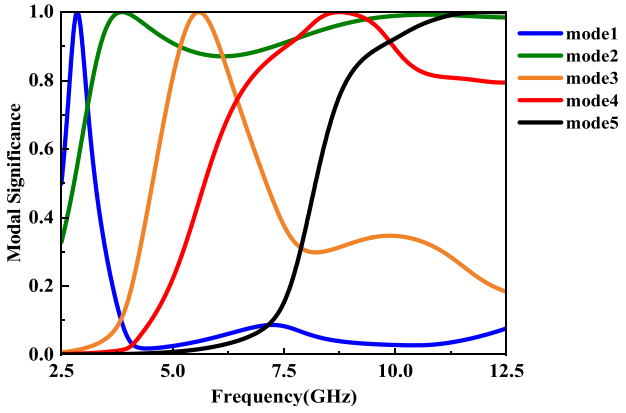

FIGURE 4. Mode analysis results for Ant 1.

Figure 3 shows strong currents near the feed line for modes 1 and 3, indicating their excitability. Mode 1 current flows from the feed point to the circular patch, whereas mode 3 current flows in the opposite direction (from patch to feed). The current of mode 4 flows from the circular patch and the feed point towards the middle of the metal trunk, and it is relatively small. The currents of mode 2 and mode 5 are nearly zero in the middle of the circular patch and the metal trunk part, and are very small near the feed point. There is a current distribution only on the ground plane, indicating that mode 2 and mode 5 are difficult to be excited. Figure 4 indicates that mode 1 resonates in the low-frequency band. Mode 3 resonates in the mid-frequency band, and mode 4 resonates at 8.75 GHz within the mid-frequency band. Mode 2 and mode 5 respectively have the potential to be-

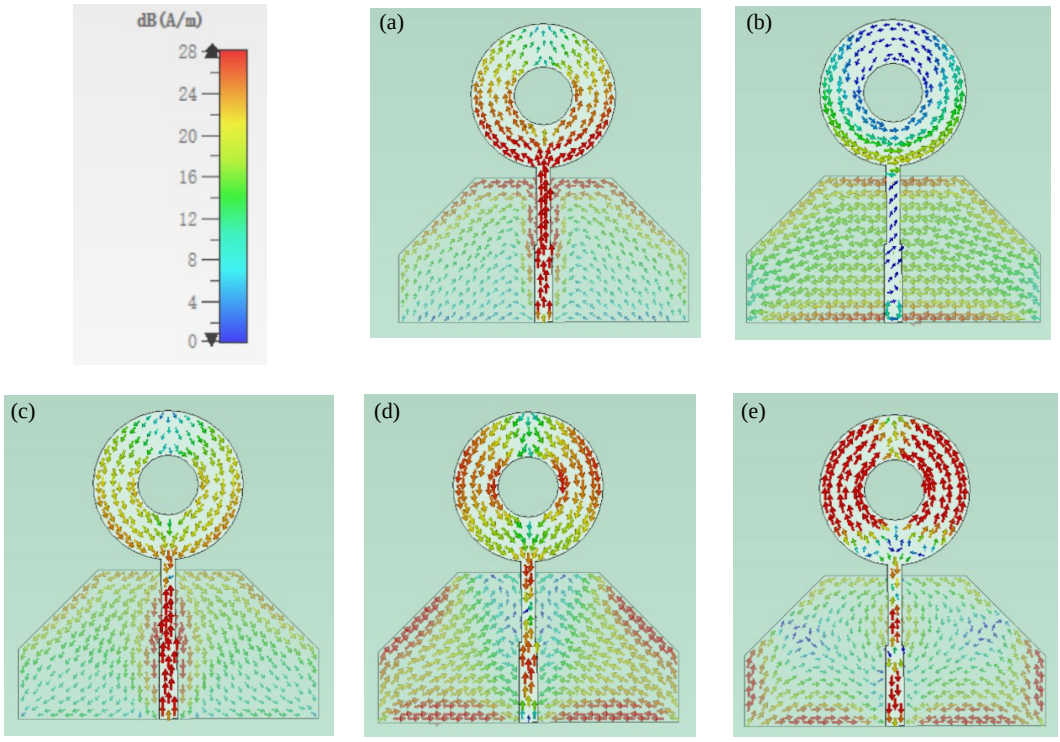

FIGURE 5. Mode current distribution of Ant 2: (a) mode 1, (b) mode 2, (c) mode 3, (d) mode 4, (e) mode 5.

come the resonant modes in the low-frequency band and high-frequency band.

To excite mode 5 and enhance its current at the patch center, the antenna structure is modified. Additionally, Figure 3 reveals mixed-mode current distributions, where the resonance points of mode 1 and mode 2 are located below 4.5 GHz, so they are main modes, while the resonance points of the other three modes are located in the middle and high frequency bands, so they are higher order modes.

A circular slot with a radius of $R_4 = 3$ mm is created in the circular portion of the patch. Simultaneously, an isosceles right triangle with a right-angled side length of 8 mm is removed from each of the left and right sides of the ground plane. The modified structure is Ant 2, as depicted in Figure 2(b).

The characteristic mode analysis of Ant 2 was performed, and the mode current distribution of Ant 2 is presented in Figure 5. It can be observed from Figure 5 that the current of mode 5 in the vicinity of the feeding point has been significantly enhanced, signifying the successful excitation of mode 5. Compared to Ant 1, currents for modes 1, 4, and 5 on the circular patch are significantly enhanced, indicating that the circular slot improves impedance matching and strengthens currents. Regarding the currents distributed on the circular patch, the current of mode 1 is primarily distributed beneath the circular patch, the current of mode 4 mainly located near the opened circular slot, and the current of mode 5 mainly distributed on the left and right sides of the circular patch. Simultaneously, the currents of mode 1, mode 2, and mode 4 on the ground plane have been considerably enhanced. Concerning the currents distributed on the ground plane, the current of mode 1 is mainly distributed on the upper side and at the corner cuts of the ground plane, the current of mode 2 mainly distributed on the upper and lower sides and at the corner cuts of the ground plane, and the current of mode 4 mainly distributed on the lower side and at the corner cuts of the ground plane. This indicates that the removed right-angled triangles have intensified the current on the ground plane. The sole deficiency is that the current of mode 2 at the feeding point remains quite small, indicating that mode 2 is still difficult to be excited.

The MS curve of Ant 2 is shown in Figure 6. It can be seen from Figure 6 that the resonant points of mode 1, mode 2, and mode 5 remain basically unchanged. The resonant point of mode 3 shifts to the right, moving from 4.94 GHz to 5.59 GHz. The resonant point of mode 4 shifts to the left, from 8.75 GHz to 8.26 GHz. The resonant point of mode 5 is 11.7 GHz, serving as the resonant mode in the high-frequency band. To excite mode 2 and make it work together with mode 1 as the reso-

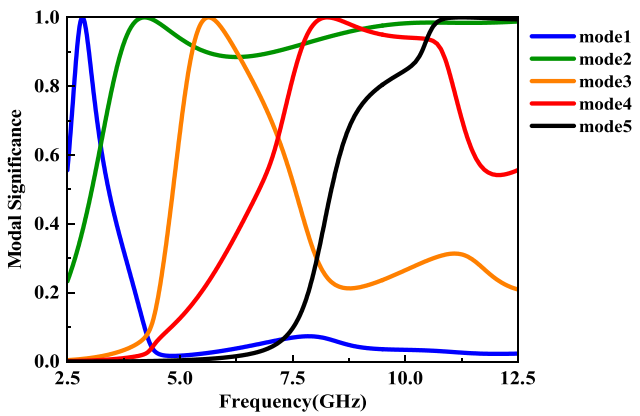

FIGURE 6. Mode analysis results for Ant 2.

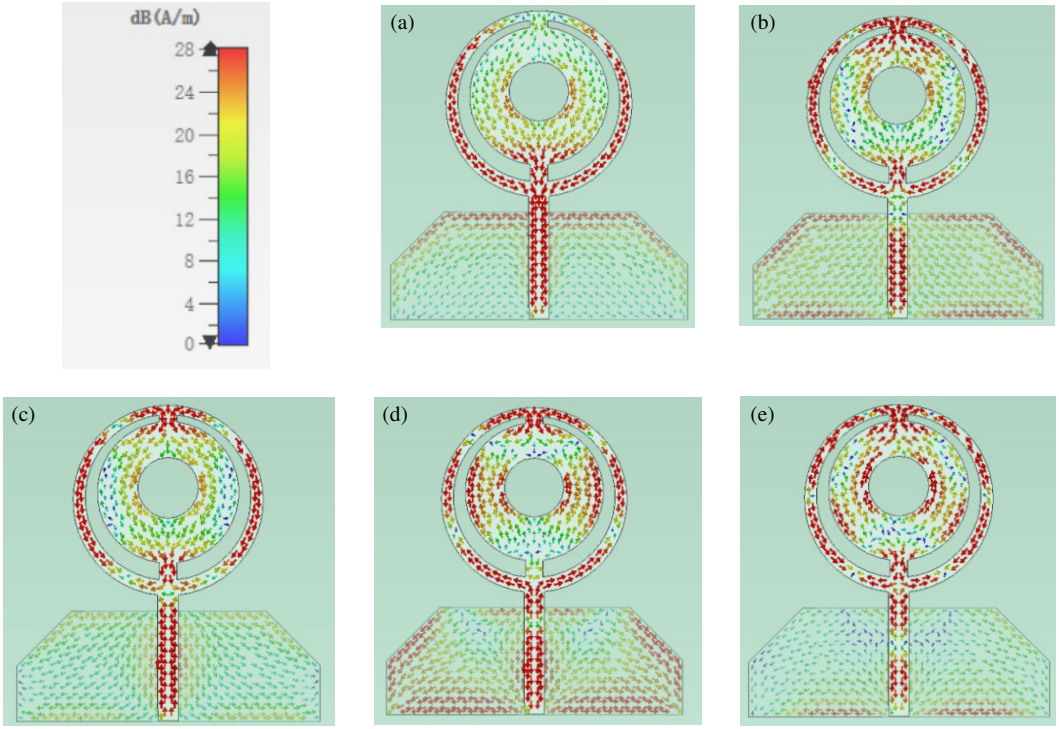

FIGURE 7. Mode current distribution of Ant 3: (a) mode 1, (b) mode 2, (c) mode 3, (d) mode 4, (e) mode 5.

nant modes in the low-frequency band, the structure of the antenna needs to be further improved. It can also be seen from Figure 5 that the resonance points of mode 4 and mode 5 gradually shift from the high-frequency band to the mid-frequency band. While the resonance points of the other modes do shift, the movement is not significant, so they do not change the current mode type.

To further enhance the matching performance and expand the frequency band coverage of the antenna, the structure of the antenna was improved. Based on Ant 2, the circular patch with a circular slot was replaced with a circular ring sleeve. The outer radius of the ring sleeve was $R_1 = 9.4$ mm, and the inner radius was $R_3 = 7$ mm. At the same time, the length of the ground plane *GND* and the length of the right-angle edge of the floor cut were optimized. The specific optimization process will be elaborated in detail in the parameter research summary. The final antenna structure after the improvement is shown in Figure 2(c), which is Ant 3.

Characteristic mode analysis was conducted on Ant 3, and the mode current distribution of Ant 3 is shown in Figure 7. As can be seen from Figure 7, the current of mode 2 is very strong near the feeding point, indicating that mode 2 has been successfully excited. Regarding the current distribution on the loop, the current of mode 1 is mainly distributed on the left and right sides of the loop and the connection with the metal main body, while the current of mode 2 is mainly distributed on the left and right sides of the loop and the upper and lower connection points between the loop and circular patch. The current distribution of mode 3 is similar to that of mode 2, but the current directions are opposite. The current of mode 4 and mode 5 is not only distributed on the loop but also in the center of the circular patch, indicating that the added loop significantly enhances the current.

The MS curve of Ant 3 is shown in Figure 8. It can be seen from Figure 8 that the resonant points of mode 2 and mode 4 remain almost unchanged, while the resonant point of mode 1 shifts to the right from 2.86 GHz to 3.7 GHz, and that of mode 3 continues to shift to the right from 5.59 GHz to 6.45 GHz. The resonant point of mode 5 shifts to the left from 11.7 GHz to 9.65 GHz. The results show that modes 1 and 2 resonate in the low-frequency band, modes 3 and 4 in the mid-frequency band, and mode 5 in the high-frequency band, with all modes effectively excited. The resonant points correspond to those of Ant 3 in Figure 9 of the next subsection. The antenna covers the frequency band of 3.04–12.5 GHz, which is basically consistent with the S parameters in Figure 9 and meets the UWB

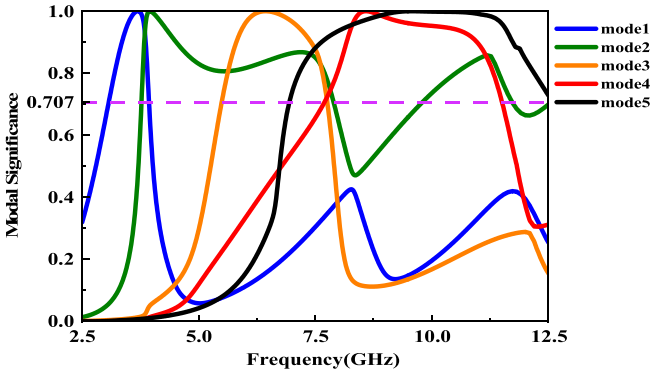

FIGURE 8. Mode analysis results for Ant 3.

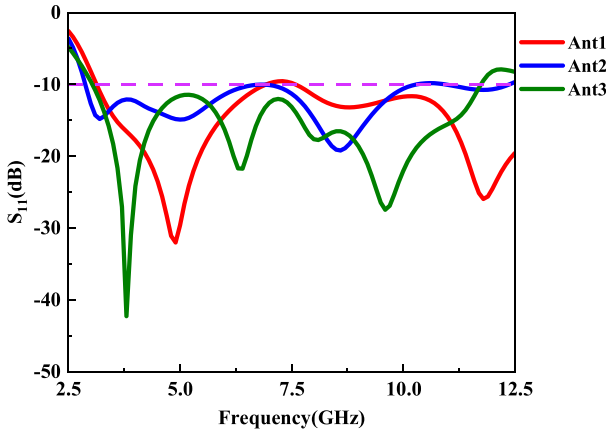

FIGURE 9. S-parameters corresponding to each process.

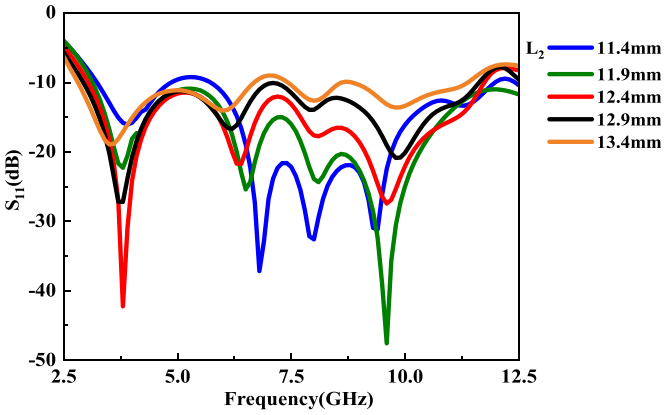

FIGURE 10. Effect of trunk length L_2 on S-parameter.

frequency requirements. It can also be known from Figure 7 that the resonance points of each mode have not changed significantly, so it can be determined that modes 1, 2, and 3 are the dominant modes, and the other two modes are the higher-order modes, which cover multiple bands through the resonance frequencies of the different modes, superimpose the bands covered by them, and obtain the UWB, which achieves the design goal of this paper.

3.2. S-Parameter Analysis of Antennas

To intuitively analyze the performance evolution during optimization and clarify the purpose of each structural change, the S-parameters of all intermediate structures are simulated and analyzed using HFSS. The results are shown in Figure 9. It can be seen from Figure 9 that the S parameters of Ant 1 are above -10 dB in the 6.93–7.58 GHz frequency band, thus not meeting the UWB requirements, and the antenna structure needs to be improved. The improved Ant 2 covers the 2.88–12.38 GHz frequency band, all of which are below -10 dB, indicating that the frequency band covered by Ant 2 meets the UWB requirements. However, the 6.5–7.0 GHz and 10.31–10.94 GHz frequency bands of Ant 2 are close to -10 dB, and the minimum S_{11} is -19.5 dB, so the antenna structure needs to be further improved. The improved Ant 3 covers the 3.03–11.75 GHz frequency band, meeting the UWB requirements, and the minimum S_{11} is -42.26 dB. Thus, it can be known that the analysis results of each antenna structure and S parameters in the process of evolving through characteristic mode analysis are consistent.

3.2.1. Research on Main Parameters of the Antenna

This study systematically investigates the influence mechanism of key structural parameters on the antenna performance, with a particular emphasis on the regulatory role of parameter variations in the working bandwidth. Through the establishment of a three-dimensional electromagnetic simulation model, the sensitive characteristics of key geometric parameters such as the main stem length of the patch (L_2), the length of the ground plane (*GND*), and the cut angle size of the ground plane (d) are examined in detail. Among them, L_2 as the core parameter of the annular radiation structure, significantly modifies the resonant characteristics of the antenna by adjusting the relative position relationship between the annular radiator and grounding structure. The parameter *GND* directly influences the electromagnetic coupling efficiency of the ground plane, while parameter d optimizes the impedance matching characteristics by controlling the current path distribution. Quantitative analysis based on the parameter scanning method demonstrates that the synergy of these three parameters is an effective regulatory mechanism for the working bandwidth of the antenna. The following sections will conduct analyses of these three parameters respectively.

As shown in Figure 10, the length L_2 of the main trunk affects the position of the loop, thereby influencing the antenna performance. When L_2 is 11.4 mm, S-parameters of the antenna are higher than -10 dB, which might be due to the mismatch between the position of the loop and the working frequency of the antenna, causing impedance mismatch and affecting the antenna performance. As L_2 increases, when it reaches 12.4 mm, S-parameters of the low-frequency resonant point become increasingly lower, indicating better performance. However, when L_2 increases to 12.9 mm, S-parameters of the mid-frequency and high-frequency resonant points become very poor. When L_2 is 13.4 mm, S-parameters of the antenna are again higher than -10 dB, indicating that the length of L_2 has a significant impact on the antenna performance and needs to be within a reasonable range to meet the UWB requirements. Therefore, after optimization, the length of L_2 is set to 12.4 mm.

As shown in Figure 11, the length of the ground plane, *GND*, has a certain impact on the S-parameters at the resonant points. When the length of *GND* is 9.9 mm, S-parameters of the antenna are greater than -10 dB, which does not meet UWB requirements. When the length of *GND* is further increased to 10.9 mm, S-parameters at the resonant points become lower and lower, indicating better performance, and the covered frequency band also becomes wider. However, when the length of *GND* is increased to 11.4 mm, although the covered frequency band is further expanded, S-parameters in the low-frequency part are higher than -10 dB. Therefore, the optimized length of the ground plane is 10.9 mm. As shown in Figure 12, the

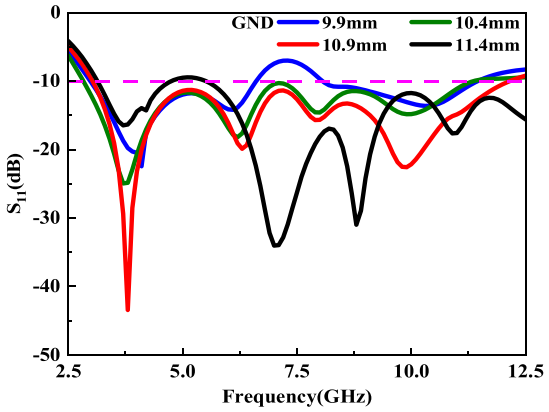

FIGURE 11. Effect of the length of the grounding plate *GND* on S-parameter.

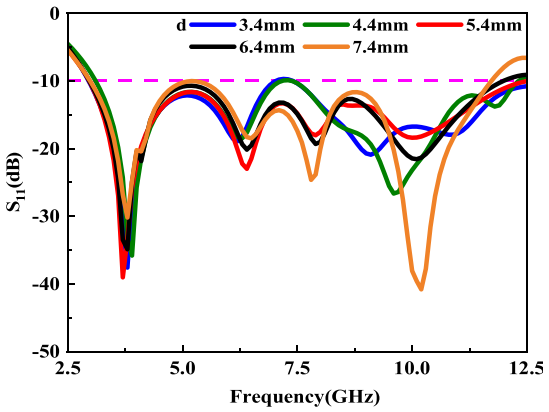

FIGURE 12. Effect of right-angled edge length d on S-parameter.

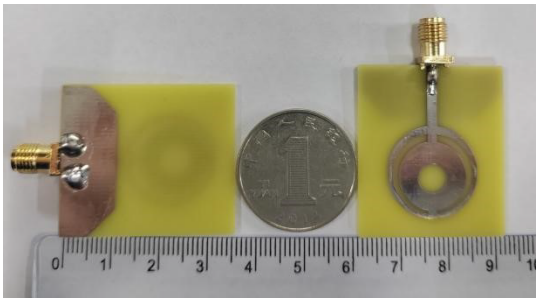

FIGURE 13. Physical structure of UWB monopole antenna.

FIGURE 14. Antenna test environment.

length d of the right-angle side of the ground plane cut corner also has a certain impact on S-parameters at the mid-frequency and high-frequency resonant points, but has no obvious effect on the low-frequency resonant point. When d increases from 3.4 mm to 5.4 mm, S-parameters in the low-frequency and mid-frequency bands become lower and lower. However, when the length of d increases to 6.4 mm or even 7.4 mm, although S-parameters in the high-frequency part become better and better, S-parameters in the low-frequency and mid-frequency parts are close to -10 dB, and the covered frequency band range becomes narrower, indicating a decline in antenna performance. This may be because as the ground plane cut corner increases, it exceeds a certain limit. Therefore, the optimized length d of the right-angle side of the ground plane cut corner is 5.4 mm.

4. RESULTS AND DISCUSSION

To verify the consistency between the performance of the UWB monopole antenna designed in this research and the simulation results, tests are conducted on the fabricated antenna prototype. As shown in the physical image of the antenna in Figure 13, the specific structural form can be seen. The test was carried out using a vector network analyzer for S-parameter measurement: the test port was connected through a coaxial cable, and the non-test ports were all connected to 50 Ω matching loads. All measurements were completed in a microwave anechoic chamber with electromagnetic shielding function, as shown in Figure 14. This test scheme effectively excluded external interference factors and ensured the accuracy of the test data.

4.1. S-Parameters

S-parameters of the UWB antenna in simulation and measurement are shown in Figure 15. From Figure 15, it can be seen that the resonant points of this antenna are 3.8 GHz, 6.4 GHz, 8.1 GHz, and 9.6 GHz. The covered frequency band is 3.03–11.75 GHz, which meets the UWB requirements. The lowest return loss is -42.26 dB, achieving the design goal. However, there is a certain deviation between the simulated results and measured data, which may be caused by the combined effect of welding errors and manufacturing errors.

As can be seen from Figure 16, within the entire working frequency band, the radiation efficiency of this antenna ranges from 65% to 85%, indicating good radiation characteristics.

4.2. Orientation Charts

The orientation charts of the E-plane and H-plane of the UWB antenna at the resonant point are measured in a microwave anechoic chamber, as shown in Figure 17. Generally speaking, the simulated results are basically consistent with the measured ones. The minor differences that exist may be due to the material properties, processing accuracy, and SMA interface welding during the antenna manufacturing process.

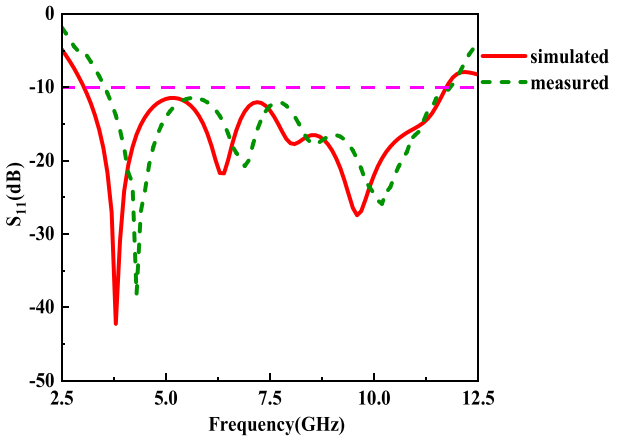

FIGURE 15. Simulated and measured S-parameters of UWB monopole antenna.

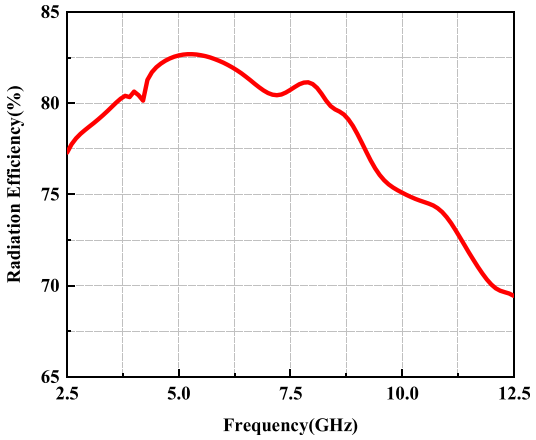

FIGURE 16. Radiation efficiency of the proposed antenna.

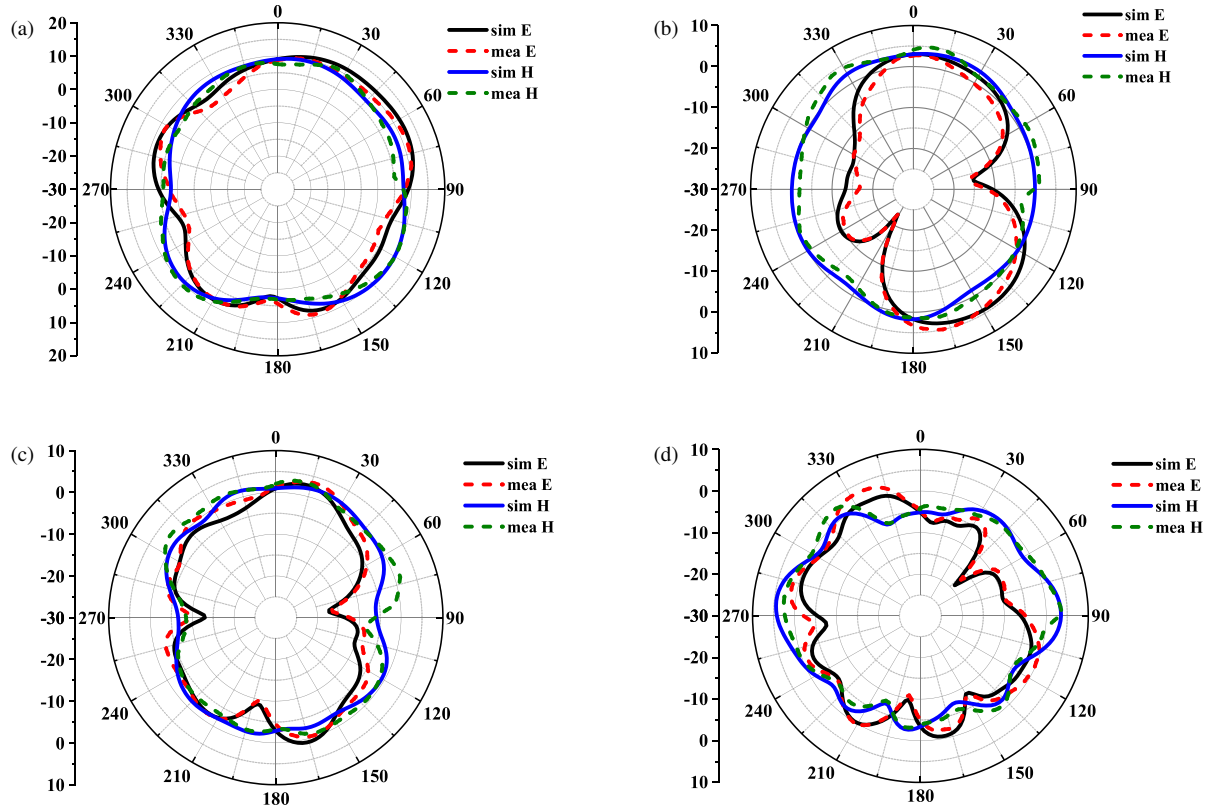

FIGURE 17. Simulated and measured orientation charts: (a) 3.8 GHz, (b) 6.4 GHz, (c) 8.1 GHz, (d) 9.6 GHz.

From Figures 17(a) and (b), it can be concluded that the H-plane pattern is approximately circular at 3.8 GHz and 6.4 GHz, indicating good omnidirectional radiation characteristics; at the same time, from Figures 17(c) and (d), it can be seen that the H-plane pattern is approximately elliptical at 8.1 GHz, indicating good directional radiation characteristics within the ranges of 0–60°, 120–240°, and 300–360°. At 9.6 GHz, it has good directional radiation characteristics within the ranges of 30–105° and 240–300°.

At 3.8 GHz, the E-plane pattern shows good performance at 30–90°, 195–240°, and 255–315°; at 6.4 GHz, the E-plane pattern resembles the digit "8"; at 8.1 GHz, the E-plane pattern radiates well at 0–60°, 105–180°, 210–255°, and 285–330°; at 9.6 GHz, the E-plane pattern shows good radiation performance in specific angle areas, indicating that the energy is concentrated in these parts, thus the entire antenna exhibits excellent directional radiation performance.

5. PERFORMANCE COMPARISON OF UWB MONOPOLE ANTENNAS

In this section, the performance of the designed antenna in this paper is compared with some proposed UWB antennas, as

TABLE 2. Performance comparison of UWB monopole antennas.

Reference	Size (mm^3)	Bandwidth (GHz)	S_{11} (dB)	Radiation Efficiency (%)
[1]	$34 \times 34 \times 1.6$	3.1–10.6	-38	-
[14]	$40 \times 36 \times 1$	2.2–3.3, 4.3–5.1, 6.3–10.8	-27	-
[19]	$50 \times 50 \times 1.575$	2.6–10.2	-35	75–80
[20]	$70 \times 70 \times 16$	2–6	-40	> 95
[21]	$35 \times 33 \times 1.6$	2.7–11	-24	75–85
[23]	$41 \times 41 \times 1$	0.609–9.105	-36	65–80
[24]	$44 \times 46 \times 1.27$	5.8–7.2	-30	83.7–98.7
Proposed antenna	$35 \times 30 \times 1.6$	3.03–11.75	-42.26	65–85

shown in Table 2. It has the smallest size and the lowest S_{11} value. Although the low-frequency bandwidth is not as wide as those in [14] and [19], the coverage in the high-frequency range is wider, and the radiation efficiency meets practical requirements. Overall, this antenna has significant advantages in terms of size, impedance bandwidth, high-frequency coverage, and low return loss. The structure is simple, and it can be concluded that this design is more suitable for compact UWB wireless communication systems.

6. CONCLUSION

This paper has designed a UWB monopole antenna using characteristic mode theory. Impedance matching is enhanced by a central circular slot and an external ring on the patch. Bandwidth expansion is achieved by optimizing the ground plane length (GND) and cut-corner dimension (d). The results show that the antenna covers the UWB frequency, with a return loss greater than -10 dB in the 3.03–11.75 GHz frequency band, and the minimum return loss is -42.26 dB. The radiation performance is good, and it can be applied to future UWB devices and wireless communication systems. The extended high-frequency coverage, reaching up to 11.75 GHz, satisfies broader UWB requirements.

ACKNOWLEDGEMENT

This work was supported by the Fund of Anhui Mining Machinery and Electrical Equipment Coordination Innovation Center (Anhui University of Science and Technology) under grant No. KSJD202406.

REFERENCES

[1] Ghahremani, M., C. Ghobadi, J. Nourinia, M. S. Ellis, F. Alizadeh, and B. Mohammadi, "Miniaturised UWB antenna with dual-band rejection of WLAN/WiMAX using slitted EBG structure," *IET Microwaves, Antennas & Propagation*, Vol. 13, No. 3, 360–366, 2019.

[2] Zhang, H., T. Sun, W. Ren, C. Yuan, and D. Chen, "A novel dual-band printed monopole antenna with modified SIR loading," *IEEE Access*, Vol. 12, 13 893–13 899, 2024.

[3] Chen, Z., J. Zeng, and J. Wang, "Compact ultrawideband H-plane horn antenna inspired by modified double-sleeve monopole," *IEEE Antennas and Wireless Propagation Letters*, Vol. 23, No. 9, 2767–2771, 2024.

[4] Guo, Z., H. Tian, X. Wang, Q. Luo, and Y. Ji, "Bandwidth enhancement of monopole UWB antenna with new slots and EBG structures," *IEEE Antennas and Wireless Propagation Letters*, Vol. 12, 1550–1553, 2013.

[5] Foudazi, A., H. R. Hassani, and S. M. A. Nezhad, "Small UWB planar monopole antenna with added GPS/GSM/WLAN bands," *IEEE Transactions on Antennas and Propagation*, Vol. 60, No. 6, 2987–2992, 2012.

[6] Nikolaou, S. and M. A. B. Abbasi, "Design and development of a compact UWB monopole antenna with easily-controllable return loss," *IEEE Transactions on Antennas and Propagation*, Vol. 65, No. 4, 2063–2067, 2017.

[7] Nie, L. Y., B. K. Lau, S. Xiang, H. Aliakbari, B. Wang, and X. Q. Lin, "Wideband design of a compact monopole-like circular patch antenna using modal analysis," *IEEE Antennas and Wireless Propagation Letters*, Vol. 20, No. 6, 918–922, 2021.

[8] Zhou, Q. L., X. Chen, and G. Fu, "A miniaturized wideband circularly polarized antenna based on tightly coupled monopole," *IEEE Antennas and Wireless Propagation Letters*, Vol. 23, No. 6, 1864–1868, 2024.

[9] Wang, X. H., H. W. Pan, L. Z. Wang, X. W. Shi, and Y. Xu, "A simple frequency- and polarization-reconfigurable bent monopole antenna based on liquid metal," *IEEE Antennas and Wireless Propagation Letters*, Vol. 22, No. 5, 950–954, 2023.

[10] Luo, Z., T. Su, and K.-D. Xu, "A single-layer low-profile dual-wideband monopolar patch antenna with shorting vias and parasitic annular sectors," *IEEE Antennas and Wireless Propagation Letters*, Vol. 22, No. 2, 432–436, 2023.

[11] Ding, A., T. H. Gan, and Z. Shen, "Design of a compact and wideband printed monopole antenna with stable omnidirectional radiation patterns," *IEEE Antennas and Wireless Propagation Letters*, Vol. 23, No. 5, 1483–1487, 2024.

[12] Hu, W., Q. Li, H. Wu, Z. Chen, L. Wen, W. Jiang, and S. Gao, "Dual-band antenna pair with high isolation using multiple orthogonal modes for 5G smartphones," *IEEE Transactions on Antennas and Propagation*, Vol. 71, No. 2, 1949–1954, 2023.

[13] Ji, F., H. Zhang, X. Xing, W. Lu, and L. Zhu, "Dual-mode resonant sectorial monopole antenna with stable backfire gain," *Chinese Journal of Electronics*, Vol. 33, No. 6, 1478–1486, 2024.

[14] Du, Y. and M. Liu, "A dual-notched ultra-wideband monopole antenna based on frequency selective surface technology," *Progress In Electromagnetics Research C*, Vol. 145, 101–105, 2024.

[15] Park, S. and K.-Y. Jung, "Novel compact UWB planar monopole antenna using a ribbon-shaped slot," *IEEE Access*, Vol. 10, 61 951–61 959, 2022.

[16] Ren, J., W. Hu, Y. Yin, and R. Fan, "Compact printed MIMO antenna for UWB applications," *IEEE Antennas and Wireless Propagation Letters*, Vol. 13, 1517–1520, 2014.

[17] Zhu, F., S. Gao, A. T. S. Ho, R. A. Abd-Alhameed, C. H. See, T. W. C. Brown, J. Li, G. Wei, and J. Xu, "Multiple band-notched UWB antenna with band-rejected elements integrated in the feed line," *IEEE Transactions on Antennas and Propagation*, Vol. 61, No. 8, 3952–3960, 2013.

[18] Schantz, H. G., "A brief history of UWB antennas," *IEEE Aerospace and Electronic Systems Magazine*, Vol. 19, No. 4, 22–26, 2004.

[19] Siddiqui, J. Y., C. Saha, and Y. M. M. Antar, "Compact dual-SRR-loaded UWB monopole antenna with dual frequency and wideband notch characteristics," *IEEE Antennas and Wireless Propagation Letters*, Vol. 14, 100–103, 2015.

[20] Saeed, M. J., M. M. Tahseen, and A. A. Kishk, "Compact multi-band omni-directional antenna for maximizing frequency coverage," *IEEE Antennas and Wireless Propagation Letters*, Vol. 24, No. 3, 597–601, 2025.

[21] Kadam, A. A. and A. A. Deshmukh, "Pentagonal shaped UWB antenna loaded with slot and EBG structure for dual band notched response," *Progress In Electromagnetics Research M*, Vol. 95, 165–176, 2020.

[22] Chen, J., M. Wen, X. He, J. Xue, and X. Chen, "Compact, UWB, dual-polarized antenna based on tightly coupling effect," *IEEE Antennas and Wireless Propagation Letters*, Vol. 23, No. 10, 3292–3296, 2024.

[23] Reyes-Vera, E., M. Arias-Correa, A. Giraldo-Muno, D. Catano-Ochoa, and J. Santa-Marin, "Development of an improved response ultra-wideband antenna based on conductive adhesive of carbon composite," *Progress In Electromagnetics Research C*, Vol. 79, 199–208, 2017.

[24] Orugu, R., M. Nesasudha, and D. K. Janapala, "A frequency tunable hexagon shaped antenna for 5.8 GHz-WiFi and sub 6-5G mobile IoT applications," in *2021 International Conference on Computer Communication and Informatics (ICCCI)*, 1–4, Coimbatore, India, 2021.

[25] Wang, Z., M. Wang, and W. Nie, "A monopole UWB antenna for WIFI 7/Bluetooth and satellite communication," *Symmetry*, Vol. 14, No. 9, 1929, 2022.

[26] Park, S. and K.-Y. Jung, "Novel compact UWB planar monopole antenna using a ribbon-shaped slot," *IEEE Access*, Vol. 10, 61 951–61 959, 2022.

[27] Gao, G., R.-F. Zhang, W.-F. Geng, H.-J. Meng, and B. Hu, "Characteristic mode analysis of a nonuniform metasurface antenna for wearable applications," *IEEE Antennas and Wireless Propagation Letters*, Vol. 19, No. 8, 1355–1359, 2020.

[28] Lin, J.-F. and Q.-X. Chu, "Increasing bandwidth of slot antennas with combined characteristic modes," *IEEE Transactions on Antennas and Propagation*, Vol. 66, No. 6, 3148–3153, 2018.

[29] Luo, Y., Z. N. Chen, and K. Ma, "Enhanced bandwidth and directivity of a dual-mode compressed high-order mode stub-loaded dipole using characteristic mode analysis," *IEEE Transactions on Antennas and Propagation*, Vol. 67, No. 3, 1922–1925, 2019.

[30] Jabire, A. H., A. Ghaffar, X. J. Li, A. Abdu, S. Saminu, M. Alibakhshikenari, F. Falcone, and E. Limiti, "Metamaterial based design of compact UWB/MIMO monopoles antenna with characteristic mode analysis," *Applied Sciences*, Vol. 11, No. 4, 1542, 2021.

[31] Abdul-Rahman, E. and D. N. Aloi, "Design of a 5G sub-6 GHz vehicular cellular antenna element with consistent radiation pattern using characteristic mode analysis," *Sensors*, Vol. 22, No. 22, 8862, 2022.

[32] Singh, H. V. and S. Tripathi, "Compact UWB MIMO antenna with cross-shaped unconnected ground stub using characteristic mode analysis," *Microwave and Optical Technology Letters*, Vol. 61, No. 7, 1874–1881, 2019.

[33] Wu, W. and Y. P. Zhang, "Analysis of ultra-wideband printed planar quasi-monopole antennas using the theory of characteristic modes," *IEEE Antennas and Propagation Magazine*, Vol. 52, No. 6, 67–77, 2010.

[34] Ren, M., J. Li, H. Zhao, and C. Xia, "A novel triband circularly polarized metasurface antenna based on characteristic mode analysis," *IEEE Antennas and Wireless Propagation Letters*, Vol. 23, No. 11, 3817–3821, 2024.

[35] Fu, C., C. Feng, W. Chu, Y. Yue, X. Zhu, and W. Gu, "Design of a broadband high-gain omnidirectional antenna with low cross polarization based on characteristic mode theory," *IEEE Antennas and Wireless Propagation Letters*, Vol. 21, No. 9, 1747–1751, 2022.

[36] Wen, D., Y. Hao, H. Wang, and H. Zhou, "Design of a wideband antenna with stable omnidirectional radiation pattern using the theory of characteristic modes," *IEEE Transactions on Antennas and Propagation*, Vol. 65, No. 5, 2671–2676, 2017.

[37] Ding, Z., Y. Liu, R. Ran, B. Wu, C. Liu, and Y. Fu, "Design of low-profile four-modes patterns metasurface antenna using characteristic mode analysis," *AEU — International Journal of Electronics and Communications*, Vol. 175, 155096, 2024.

[38] Khan, M. and M. Chowdhury, "Analysis of modal excitation in wideband slot-loaded microstrip patch antenna using theory of characteristic modes," *IEEE Transactions on Antennas and Propagation*, Vol. 68, No. 11, 7618–7623, 2020.

[39] Peñafiel-Ojeda, C. R., C. E. Andrade, R. Baez-Egas, and V. Garcia-Santos, "An ultrawideband printed monopole antenna analyzed with the theory of characteristic modes," *IEEE Latin America Transactions*, Vol. 20, No. 6, 948–954, 2022.

[40] Zhao, X., S. P. Yeo, and L. C. Ong, "Planar UWB MIMO antenna with pattern diversity and isolation improvement for mobile platform based on the theory of characteristic modes," *IEEE Transactions on Antennas and Propagation*, Vol. 66, No. 1, 420–425, 2018.